Journal of Power Sources 266 (2014) 170–174

Contents lists available at ScienceDirect

Journal of Power Sources

journal homepage: www.elsevier.com/locate/jpowsour

Short communication

Characterization tests for plug-in hybrid electric vehicle application of graphite/$LiNi_{0.4}Mn_{1.6}O_4$ cells with two different separators and electrolytes

C. Arbizzani, F. De Giorgio, M. Mastragostino*

Alma Mater Studiorum Università di Bologna, Dipartimento di Chimica "Giacomo Ciamician", Via Selmi 2, 40126 Bologna, Italy

HIGHLIGHTS

- Graphite/LNMO cells were tested by protocol for plug-in HEV application.
- Cell assemblies with two different separators were tested in two electrolytes.
- PVdF-based separator had strong impact on high-rate functioning LIB for PHEVs.

ARTICLE INFO

Article history:
Received 11 March 2014
Received in revised form
10 April 2014
Accepted 3 May 2014
Available online 14 May 2014

Keywords:
High-voltage lithium-ion battery
$LiNi_{0.4}Mn_{1.6}O_4$
LNMO
PHEV
Plug-in HEV test
PVdF separator

ABSTRACT

The paper reports and discusses the results of electrochemical tests carried out according to the DOE Battery Test Manual for plug-in Hybrid Electric Vehicles (PHEVs) on laboratory high-voltage graphite/$LiNi_{0.4}Mn_{1.6}O_4$ cells with electrode formulation and mass-loading suitable for scale-up, and mixed ethylene carbonate–dimethyl carbonate with two diverse lithium salts, lithium tris(pentafluoroethyl) trifluorophosphate and $LiPF_6$, as electrolytes. The cells, assembled with two different separators, a polypropylene monolayer separator (Celgard®2400) and a reinforced polyvinylidene fluoride macroporous membrane (PVdF-NCC), were also tested by deep charge/discharge cycles. The results show the strong impact of the separator on high-rate cell functioning in PHEVs.

1. Introduction

The worldwide demand for clean, low-fuel-consuming transport has promoted the development of safe, high-energy and power lithium-ion batteries for hybrid electric vehicles (HEVs) in the last ten years. The performance requirement for the battery system depends on the level of power-train hybridization and on the range of the electric driving. Power-assist HEVs with optimized fuel consumption and a short electric driving range are already marketed by several car manufacturers [1]. In power-assist HEVs the battery system operates in charge-sustaining (CS) mode via a dynamic functioning with shallow charge–discharge cycles around a constant state of charge. The battery discharges to provide extra power during vehicle acceleration and recovers energy from regenerative braking or from the internal combustion engine.

The electric driving range in the plug-in HEVs (PHEVs) is greater than in power-assist HEVs. The energy to drive the vehicle also comes from the battery which is recharged by the electric-grid. There are two battery operation modes: i) charge-depleting (CD) with a net decrease of the state of charge during electric propulsion of the vehicle, and ii) charge-sustaining (CS), which is similar to that of the power-assist HEV. While the power demand for the battery systems is thus almost the same for HEVs and PHEVs, the energy needed by the latter, which also operates in depleting-mode, is significantly higher. The power-to-energy ratio targets set by US Department of Energy (DOE) are 13 for minimum PHEV and 83 for minimum power-assist HEV [2,3]. Although high-energy battery pack is an issue that is still under study as well as battery safety and costs, and high-voltage lithium-ion batteries of different chemistry are under investigation, some PHEVs are already on the market.

* Corresponding author.
E-mail address: marina.mastragostino@unibo.it (M. Mastragostino).

http://dx.doi.org/10.1016/j.jpowsour.2014.05.016
0378-7753/

High-voltage graphite/$LiNi_{0.4}Mn_{1.6}O_4$ cells with reinforced polyvinylidene fluoride macroporous separator (PVdF-NCC) were recently tested against cells with commercial polypropylene monolayer (Celgard®2400) according to FreedomCAR-DOE protocols for power-assist HEV [4], and several PVdF macroporous separators were investigated in high charge-rate $Li_4Ti_5O_{12}/LiMn_2O_4$ cells and compared to commercial polyolefin separators [5].

The present paper reports and discusses the results of electrochemical tests carried out according to DOE protocols for PHEV application [3], as well as of deep charge/discharge cycles on graphite/$LiNi_{0.4}Mn_{1.6}O_4$ cells featuring electrodes of optimized formulation and mass-loading suitable for scale-up of batteries for PHEV [6], two different separators (Celgard®2400 and PVdF-NCC) and ethylene carbonate–dimethyl carbonate with different lithium salts as electrolytes.

2. Experimental

Full cells were assembled with positive and negative electrodes prepared by pre-industrial pilot lines and provided by CEA-LITEN (Grenoble, France). Two assemblies were tested: one with a commercial polypropylene separators (Celgard®2400, 25 μm), and the other with polyvinylidene fluoride (PVdF)-nano crystalline cellulose (NCC) reinforced membranes (23–28 μm) prepared by a phase-inversion process [7] with 9–15% NCC content and provided by INP-LEPMI (Grenoble, France). Electrodes and separators were developed within the 7th European Framework Programme, "Advanced Fluorinated Materials for High Safety, Energy and Calendar Life Lithium Ion Batteries" (AMELIE) Project.

The positive electrode composition (in wt%) was 92% $LiNi_{0.4}Mn_{1.6}O_4$ (LNMO, CEA) [8], 4% Super C65 (TIMCAL) conductive carbon and 4% PVdF (Solef®5130, Solvay) binder, and the negative electrode composition was 91% graphite (SLA-1025, Superior Graphite Co.), 3% PureBLACK™ (Superior Graphite, Co.) conducting additive and 6% PVdF (Solef®5130, Solvay). The active material mass-loading for single-face electrodes was 21.3 mg cm^{-2} for the positive and 8.7 mg cm^{-2} for the negative electrode in order to have a reversible capacity ratio equal to 1 between the two electrodes and to provide 2–3 mAh cm^{-2}. The 0.64 cm^2 electrodes were dried before use and cell assembly was performed in a MBraun Labmaster SP glove box (water and oxygen content < 0.1 ppm) using as electrolytes ethylene carbonate (EC):dimethyl carbonate (DMC) 1:1–1 M lithium tris(pentafluoroethyl)trifluorophosphate (LF30, Merck, water ≤ 20 ppm and HF content ≤ 50 ppm) with additives and EC:DMC 1:1–1 M $LiPF_6$ (LP30, Merck, water ≤ 20 ppm and HF content ≤ 50 ppm) with additives. The additives were monofluoroethylene carbonate (F_1EC, Solvay Fluor, purity ≥ 99.9 wt%, water and HF content ≤ 20 ppm) and succinic anhydride (SA, Sigma–Aldrich, purity ≥ 99%), used as received, and their respective amounts in the electrolyte solutions were 1.6 wt% and 2 wt%.

The electrochemical tests on the full cells were performed with a Swagelok™-type cells in two-electrode configuration at 30 °C in a Memmert IPP 200 oven using a Biologic VMP multichannel potentiostat/galvanostat. The cells had a Li reference electrode to check the potential of each electrode. Impedance spectroscopy measurements were carried out in open circuit conditions using a Solartron SI 1255 frequency response analyzer coupled with a 273 A PAR potentiostat/galvanostat. An ac amplitude of 5 mV was used, and data were collected taking 10 points per decade in the range 10 kHz–100 mHz.

3. Results and discussion

Electrochemical tests by the FreedomCAR-DOE protocols for plug-in HEV application [3] were performed on graphite/LNMO cells with Celgard®2400 or PVdF-NCC separators. In the last few years PVdF-based separators have been the focus of much interest, as reviewed by Costa et al. in ref. [9], for their interesting properties like high dipolar moment, high dielectric constant, tailored porosity, chemical and electrochemical stability in cathodic environment and good contact with electrodes. PVdF-NCC was developed in the frame of the European Project AMELIE and its properties were reported and compared with Celgard®2400 in ref. [4]. Graphite/LNMO cells were assembled with two different electrolytes, LF30 and LP30 with additives (1.6 wt% F_1EC & 2 wt% SA), which form SEI on the anode and protect the cathode [10,11]. Despite the most promising characteristics of LF30 with respect to that of LP30 for high-voltage cells due to the higher stability of lithium tris(pentafluoroethyl) trifluorophosphate than $LiPF_6$ [4,10,12], we tested cells with both electrolytes because the former is no longer commercialized. The results are compared to the end-of-life (EOL) targets set by DOE for the different PHEV types shown in Table 1. Given that the targets are referred to the total battery pack, the specific values calculated by dividing the targets by the maximum weights of the battery pack are also reported in the Table. The tests for PHEV included a static capacity test (SCT) at constant discharge current to measure battery energy, and hybrid pulse power characterization (HPPC) with 10 s discharge and regenerative pulses to determine the battery's dynamic power capability.

Fig. 1 shows the results of SCT on the cells, over the last discharge of three cycles between 3.5 V and 4.95 V at 2C effective rate corresponding to a discharge power ≥10 kW referred to minimum PHEV with 60 kg battery pack (10 and 16 kW for cells in LP30-additives with Celgard and PVdF-NCC, respectively). The cumulative specific energy values at different DOD in the Figure refer to battery weight calculated as twice the composite electrode weight of both electrodes in order to include the weight contribution of all the other battery components after ref. [13]. Hereinafter the specific parameters (energy and power) are calculated in the same manner and the indications LF30 and LP30 are used, although these electrolytes include the two additives. As expected from refs. [4,10], the cumulative energies removed from the cells with LF30 at 100% DOD (E_{SCT}) are higher than those removed from cells with LP30, with the highest values for the cells with PVdF-NCC; the values, expressed in Wh kg^{-1}, were 141 and 132 for PVdF-NCC cells in LF30 and LP30, respectively, and 111 and 79 for Celgard®2400 cells.

The HPPC tests that incorporate a 10 s discharge pulse at 5C, 40 s rest and 10 s regenerative pulse at a current which is 75% of the discharge pulse current were carried out at different depths of discharge (DOD) from 10% to 90%, separated by 10% DOD steps (performed in the same condition of the SCT) and 1 h of rest time.

Table 1
Energy storage system performance targets for plug-in HEVs.

Characteristics at EOL (end-of-life)	Unit	Minimum PHEV	Medium PHEV	Maximum PHEV
Ref. equivalent electric range	miles	10	20	40
Peak discharge pulse power (10 s)	kW	45	37	38
	W kg^{-1}	750	529	317
Peak Regen pulse power (10 s)	kW	30	25	25
	W kg^{-1}	500	357	208
Available energy for CD (charge-depleting) mode, 10 kW rate	kWh	3.4	5.8	11.6
	Wh kg^{-1}	56.7	82.9	96.7
Available energy for CS (charge-sustaining) mode, 10 kW rate	kWh	0.5	0.3	0.3
	Wh kg^{-1}	8.3	4.3	2.5
Maximum system weight	kg	60	70	120

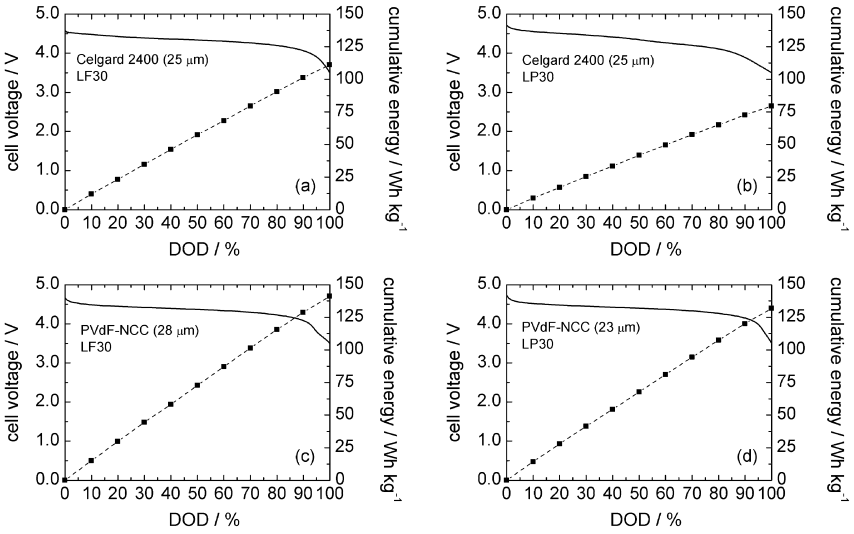

Fig. 1. Discharge voltage profile (solid line) and cumulative specific energy (dashed line) at 2C effective rate at different DOD of the cells with (a) Celgard and LF30, 3.03 mA cm^{-2}, (b) Celgard and LP30, 2.12 mA cm^{-2}, (c) PVdF-NCC and LF30, 3.85 mA cm^{-2}, (d) PVdF-NCC and LP30, 3.55 mA cm^{-2}.

Fig. 2 shows, as an example, the HPPC voltage profile of the cell with PVdF-NCC separator and LP30 along the sequence from 10% to 90% DOD with discharge pulses at 5C (8.88 mA cm^{-2}); the plot also shows the voltage during the rest time before the beginning of the test. The HPPC test ends before 90% DOD if the cell voltage exceeds the selected V_{max} value, in this case V_{max} = 5.0 V, for the cell in regenerative pulse and V_{min} = 0.55 V_{max} in discharge pulse. The inset in the Figure displays the magnification of the pulses at 10% DOD to mark the cell voltage values just before the discharge and regenerative pulses, V_0 and V_2, and those at the end of these pulses, V_1 and V_3, which are used as in ref. [3] to calculate at each %DOD the discharge and regenerative pulse resistances, R_{dis} and R_{reg},

$$R_{dis} = (V_1 - V_0)/I_{dis} \quad (1)$$

and

$$R_{reg} = (V_3 - V_2)/I_{reg} \quad (2)$$

and then, the discharge and regenerative pulse power, P_{dis} and P_{reg},

$$P_{dis} = V_{min}(V_0 - V_{min})/R_{dis} \quad (3)$$

and

$$P_{reg} = V_{max}(V_{max} - V_2)/R_{reg} \quad (4)$$

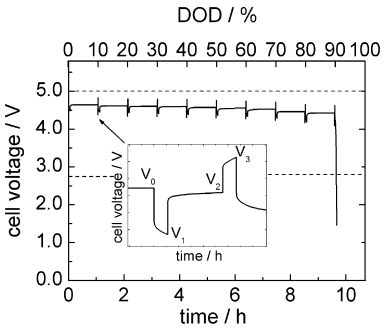

Fig. 2. Cell voltage profile over HPPC at 5C of the cell with PVdF-NCC separator and LP30. In the inset, the magnification of the discharge and regenerative pulses at 10% DOD.

The R_{dis} and R_{reg} values, shown in Fig. 3, of the cells with PVdF-NCC separator in both electrolytes are lower than those with Celgard®2400 and can partly explain the higher E_{SCT} values of the former cells. Furthermore, cells with Celgard separator provide significantly lower E_{SCT} value in LP30 than in LF30 despite the fact that the resistances are almost the same in both electrolytes. Presumably, the presence in LF30 of lithium tris(pentafluoroethyl)trifluorophosphate, which is more stable than $LiPF_6$ toward hydrolysis and oxidation, is crucial for the stability of the charged cathode when Celgard separator is used.

Fig. 4 shows the discharge and regenerative pulse power values estimated at different DOD from 5C HPPC tests *vs.* energy removed at the 2C effective rate (from SCT in Fig. 1) for the cells with both separators and electrolytes. The dashed horizontal line on the *y*-axes identifies the discharge and regenerative DOE power goals for the minimum PHEV (0.750 kW kg^{-1} and 0.500 kW kg^{-1}), and the difference in the removed energy between the two vertical lines at

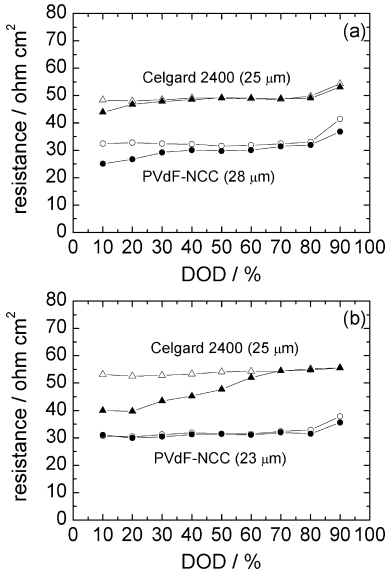

Fig. 3. Discharge (empty symbol) and regenerative (full symbol) pulse resistances *vs.* DOD% from 5C HPPC on cells with PVdF-NCC and Celgard®2400 separators and LF30 (a) and LP30 (b).

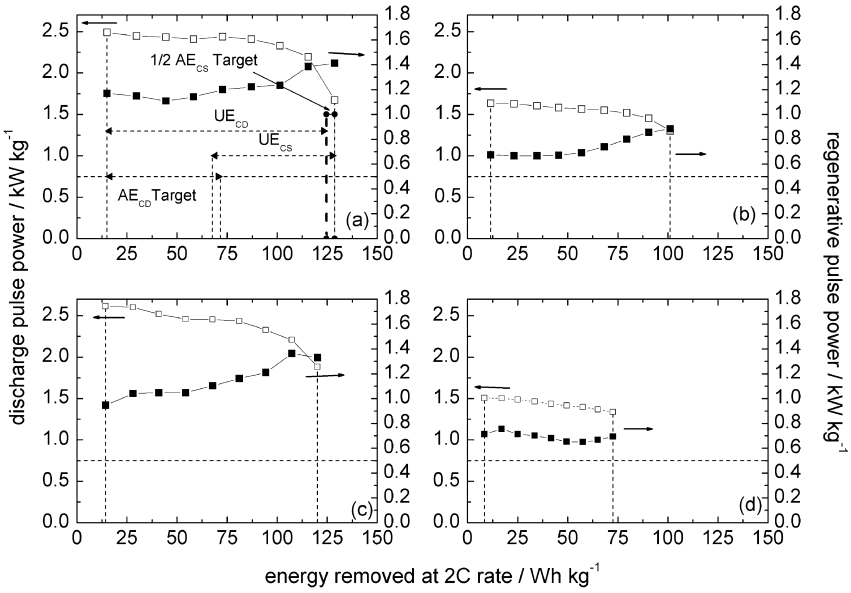

Fig. 4. Discharge (empty symbol) and regenerative (full symbol) pulse power from 5C HPPC tests on cells with PVdF-NCC (a, c) or Celgard®2400 (b, d) separator and LF30 (a, b) or LP30 (c, d).

90% and 10% DOD corresponds to the available energy of the battery system at the power targets. Taking into account the DOE energy targets for CS and CD operation modes ($AE_{CS\ Target}$ and $AE_{CD\ Target}$) reported in Table 1, the useable energy (UE) for each mode, UE_{CS} and UE_{CD}, and the useable energy margin (UE_M) can be estimated as in ref. [3] by the following equations:

$$UE_{CS} = (E_{90\%DOD} - E_{10\%DOD}) - (AE_{CD\ Target} - 1/2AE_{CS\ Target}) \quad (5)$$

$$UE_{CD} = (E_{90\%DOD} - E_{10\%DOD}) - 1/2AE_{CS\ Target} \quad (6)$$

$$UE_M = (UE_{CD} - AE_{CD\ Target}) = (UE_{CS} - AE_{CS\ Target}) \quad (7)$$

If the HPPC test ends before 90% DOD, the first term in the UE_{CS} and UE_{CD} has to be substituted with the corresponding energy value.

Given that the battery has to meet the DOE targets at the end-of-life for CS and CD modes reported in Table 1, the decrease of energy and power occurring over cycling and calendar life requires some energy margin. Thus, the margin value at the beginning of battery life must be sufficiently high, 20–30% of the $AE_{CD\ Target}$.

Table 2 summarizes the experimental E_{SCT}, UE_{CD}, UE_{CS} and UE_M values for the cells with the two separators and electrolytes, as well as $AE_{CS\ Target}$ and $AE_{CD\ Target}$ for different PHEV types.

The data in Table 2 clearly show that values of usable energy for cells in LF30 with PVdF-NCC assure some margin even when Maximum PHEV targets are considered. By contrast, cells with Celgard separator display a usable energy value that assures a significant UE_M only for Minimum PHEV. While the change of electrolyte from LF30 to LP30 does not significantly modify the performance of cells with PVdF-NCC, it has a notable effect on cells with Celgard, which meet only the target for Minimum PHEV with an unsatisfactory UE_M value, i.e. more than 10 times lower than that of cells with PVdF-NCC.

To further investigate the beneficial impact of the PVdF-NCC separator with respect to the Celgard on the high-rate performance of graphite/LNMO cells, 100 charge–discharge galvanostatic cycles between 3.5 V and 4.95 V were carried out at 1C effective rate on cells with LF30 (1.89 and 1.67 mA cm^{-2} for cells with PVdF-NCC and Celgard, respectively). These cells, which at low current density (0.300 mA cm^{-2}) delivered almost the same capacity (120 and 115 mAh g$^{-1}_{LNMO}$) and at the first 1C cycle delivered 108 and 93 mAh g$^{-1}_{LNMO}$, respectively, displayed a very different cycling stability as shown in Fig. 5, which reports the voltage profile of the 1st and 100th cycle and the capacity values normalized to initial capacity delivered at different cycles. Unlike cells with PVdF-NCC, those with Celgard showed a rapid decrease of capacity over cycling; galvanostatic charges followed by 1 h constant voltage charges at 4.95 V improved capacities but worsened coulombic efficiency without the cells reaching the capacity values of those with PVdF-NCC (data not shown). Given that the nickel oxidation potential of LNMO is as high as 4.75 V *vs.* Li, and the cells were charged up to 4.95 V, the findings suggest that higher ohmic drops in the

Table 2
Experimental E_{SCT}, UE_{CD}, UE_{CS} and UE_M values of full cells with different separators and electrolytes for different PHEV types. The DOE energy targets AE_{CS} and AE_{CD} are in the last row.

Plug-in SCT&HPPC tests	E_{SCT}	Minimum PHEV					Medium PHEV					Maximum PHEV				
		UE_{CD}	UE_{CS}	UE_M	AE_{CD}	AE_{CS}	UE_{CD}	UE_{CS}	UE_M	AE_{CD}	AE_{CS}	UE_{CD}	UE_{CS}	UE_M	AE_{CD}	AE_{CS}
	Wh kg^{-1}	Wh kg^{-1}					Wh kg^{-1}					Wh kg^{-1}				
LF30 − 1.6% F_1EC − 2% SA																
PVdF-NCC (28 μm)	141	110	61	53			112	33	29			113	18	16		
Celgard®2400 (25 μm)	111	86	37	29			88	9	5			89	–	–		
LP30 − 1.6% F_1EC − 2% SA																
PVdF-NCC (23 μm)	132	102	53	45			104	25	21			105	10	8		
Celgard®2400 (25 μm)	79	60	12	3			62	–	–			63	–	–		
DOE energy targets					57	8				83	4				97	3

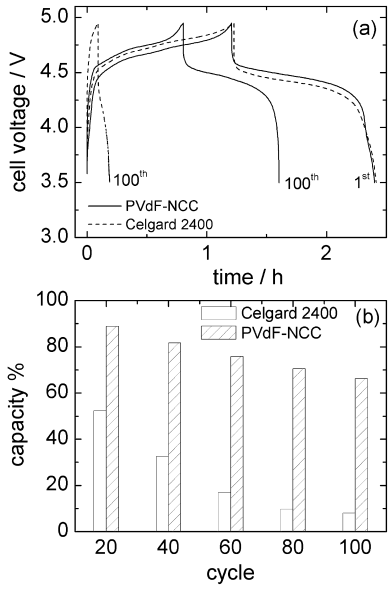

Fig. 5. (a) Voltage profiles of the 1st and 100th cycle and (b) capacity values (normalized to initial capacity) delivered at different cycles at 1C effective rate by cells with PVdF-NCC and Celgard®2400 separators with LF30.

Table 3
Internal resistance (Z_{re}) at 1 Hz of cells graphite/LNMO with PVdF-NCC and Celgard separators after the first cycle at C/10 and after 100 cycles at 1C (discharge state).

	PVdF-NCC (28 μm), ohm cm^2	Celgard®2400 (25 μm), ohm cm^2
After 1st cycle at C/10	35.0	69.5
After 100 cycles at 1C effective rate	37.6	120.0

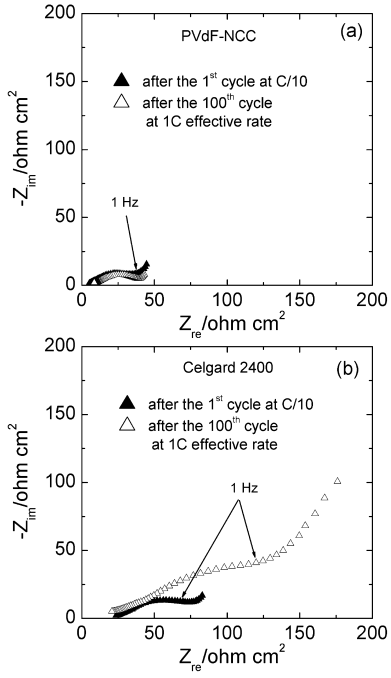

Fig. 6. Impedance spectra in the range 10 kHz–0.1 Hz of cells with (a) PVdF-NCC and (b) Celgard®2400 separators with LF30 after the first low current cycle and at the end of the 100th cycle at 1C effective rate.

Celgard cells than in the PVdF-NCCs provided lower states of charge for the former. This is supported by resistance values from HPPC tests and validated by impedance spectroscopy data at 1 Hz collected on the cells after the first low current cycle and at the end of 100 cycles at 1C as shown in Table 3, where the resistance of the PVdF-NCC cell is initially lower and remains more stable over cycling than that of the Celgard cell. The corresponding impedance spectra are shown in Fig. 6. These results confirm the beneficial impact of PVdF-based separator on high-voltage lithium-ion cells functioning at high-rate in PHEV application. The advantage of this separator can be ascribed, in addition to its lower MacMullin number than polyolefin commercial separators [4,5], to a better contact between PVdF-NCC and electrodes which include PVdF binder, a contact that in turn provides a lower, more stable resistance.

4. Conclusions

The results of the electrochemical tests on high-voltage laboratory graphite/LNMO cells with optimized electrode formulation and mass electrode loading suitable for scale-up of batteries for the high-energy demanding plug-in applications show the strong effect of the separator on cell performance. Unlike cells with Celgard®2400, which displayed usable energy values with satisfactory energy margin only for Minimum PHEV in LF30, cells with PVdF-NCC macroporous membrane displayed in both LF30 and LP30 usable energy values exceeding the targets even for Medium PHEVs with margins of 35% and 25%, respectively. The higher energy values in LF30 than in LP30 evince the need for new fluorinated salts and/or solvents, given that EC:DMC-lithium tris(-pentafluoroethyl)trifluorophosphate is no longer commercialized.

Acknowledgments

The "Advanced Fluorinated Materials for High Safety, Energy and Calendar Life Lithium Ion Batteries" (AMELIE) Project n. 265910 was funded by the 7th European Framework Programme (FP7-Transport). The authors thank L. Picard and G. Yildirim (CEA-LITEN), J.-Y. Sanchez, F. Alloin and M. Bolloli (INPG-LEPMI) for providing some cell components, all the Project Partners for the useful discussions and UE for financial support.

References

[1] State of the Plug-in Electric Vehicle Market, Electrification Coalition, PricewaterhouseCoopers, July 25, 2013 (access 23.01.14), http://www.pwc.com/gx/en/automotive/industry-publications-and-thought-leadership/state-of-the-plug-in-electric-vehicle-market.jhtml.
[2] FreedomCAR Battery Test Manual for Power-Assist Hybrid Electric Vehicles, October 2003.
[3] Battery Test Manual for Plug-In Hybrid Electric Vehicles, U.S. Department of Energy, December 2010. Vehicle Technologies Program, Revision 2.
[4] C. Arbizzani, F. Colò, F. De Giorgio, M. Guidotti, M. Mastragostino, F. Alloin, M. Bolloli, Y. Molméret, J.-Y. Sanchez, J. Power Sources 246 (2014) 299–304.
[5] D. Djian, F. Alloin, S. Martinet, H. Lignier, J. Power Sources 187 (2009) 575–580.
[6] W. Lu, A. Jansen, D. Dees, P. Nelson, N.R. Veselka, Gary Henriksen, J. Power Sources 196 (2011) 1537–1540.
[7] J. Saunier, F. Alloin, J.-Y. Sanchez, G. Caillon, J. Power Sources 119-121 (2003) 454–459.
[8] S. Patoux, L. Daniel, C. Bourbon, H. Lignier, C. Pagano, F. Le Cras, S. Jouanneau, S. Martinet, J. Power Sources 189 (2009) 344–352.
[9] C.M. Costa, M.M. Silva, S. Lanceros-Méndez, RCS Adv. 3 (2013) 11404–11417.
[10] C. Arbizzani, F. De Giorgio, L. Porcarelli, M. Mastragostino, V. Khomenko, V. Barsukov, D. Bresser, S. Passerini, J. Power Sources 238 (2013) 17–20.
[11] V. Tarnopolskiy, J. Kalhoff, M. Nádherná, D. Bresser, L. Picard, F. Fabre, M. Rey, S. Passerini, J. Power Sources 236 (2013) 39–46.
[12] M. Schmidt, U. Heider, A. Kuehner, R. Oesten, M. Jungnitz, N. Ignat'ev, P. Sartori, J. Power Sources 97–98 (2001) 557–560.
[13] S.G. Stewart, V. Srinivasan, J. Newman, J. Electrochem. Soc. 155 (2008) A664–A671.